Korean Journal of Remote Sensing, Vol.21, No.3, 2005, pp.173~188

Derivation and Comparison of Narrow and Broadband Algorithms for the Retrieval of Ocean Color Information from Multi-Spectral Camera on Kompsat-2 Satellite

Yu-Hwan Ahn†, Palanisamy Shanmugam, Joo-Hyung Ryu, and Jeong-Eon Moon

Korea Ocean Research and Development Institute

Abstract : The present study aims to derive and compare narrow and broad bandwidths of ocean color sensor's algorithms for the study of monitoring highly dynamic coastal oceanic environmental parameters using high-resolution imagery acquired from Multi-spectral Camera (MSC) on KOMPSAT-2. These algorithms are derived based on a large data set of remote sensing reflectances (R_{rs}) generated by using numerical model that relates $b_b/(a + b_b)$ to R_{rs} as functions of inherent optical properties, such as absorption and backscattering coefficients of six water components including water, phytoplankton (chl), dissolved organic matter (DOM), suspended sediment (SS) concentration, heterotropic organism (he) and an unknown component, possibly represented by bubbles or other particulates unrelated to the first five components. The modeled R_{rs} spectra appear to be consistent with in-situ spectra collected from Korean waters. As Kompsat-2 MSC has similar spectral characteristics with Landsat-5 Thematic Mapper (TM), the model generated Rrs values at 2 nm interval are converted to the equivalent remote sensing reflectances at MSC and TM bands. The empirical relationships between the spectral ratios of modeled R_{rs} and chlorophyll concentrations are established in order to derive <chl> algorithms for both TM and MSC. Similarly, <SS> algorithms are obtained by relating a single band reflectance (band 2) to the suspended sediment concentrations. These algorithms derived by taking into account the narrow and broad spectral bandwidths are compared and assessed. Findings suggest that there was less difference between the broad and narrow band relationships, and the determination coefficient (r^2) for log-transformed data [<chl> N = 500] was interestingly found to be $r^2 = 0.90$ for both TM and MSC. Similarly, the determination coefficient for log-transformed data [<SS> N = 500] was 0.93 and 0.92 for TM and MSC respectively. The algorithms presented here are expected to make significant contribution to the enhanced understanding of coastal oceanic environmental parameters using Multi-spectral Camera.

Key Words : Ocean color, Multi-Spectral Camera, Landsat-TM, Case-1 and Case-II waters, R_{rs} Model and Spectral Band Model.

1. Introduction

The color of the ocean measured from space, which can be determined by the reflectance ratio of upwelling (E_u) to downwelling irradiance (E_d) just beneath the

Received 2 March 2005; Accepted 10 June 2005.

† Corresponding Author: Y. – H. Ahn (yhahn@kordi.re.kr)

surface, provides information on the abundance of the coastal and open oceanic water constituents such as phytoplankton, dissolved organic matter and suspended particulate materials. These informations can have immense value to investigate the optical properties of upper ocean layers, biological productivity, global carbon and biogeochemical cycle in the oceans. The launch of Coastal Zone Color Scanner (CZCS) by National Aeronautics and Space Administration (NASA) on the Nimbus-7 satellite in 1978 has made a significant contribution to the ocean color community to study the spatial and temporal evolution of phytoplankton distribution in the open oceanic waters, characterizing the highly dynamic features such as eddies, meanders and variability of ocean circulation patterns at local and regional scales (Gordon *et al.*, 1980; Barale and Trees, 1987; Abbott and Chelton, 1991). The end of CZCS in 1986 has resulted many other ocean observation radiometers of improved spatial and spectral characteristics, which have been deployed on space borne satellites abroad to study more precisely these aspects in the oceans. These ocean color instruments include Sea-viewing Wide Field-of-View Sensor (SeaWiFS), Ocean Color and Temperature Scanner (OCTS), Modular Optoelectronic Scanner (MOS), Polarization and Directionality of Earth Reflectances (POLDER), Moderate Resolution Imaging Spectrometer (MODIS), Medium Resolution Imaging Spectrometer (MERIS), Ocean Scanning Multispectral Imager (OSMI), Ocean Color Monitor (OCM) and Global Line Imager (GLI). In order to acquire high temporal ocean color imagery, the first Geostationary Ocean Color Imager (GOSI) on Communication Ocean Meteorological Satellite (COMS) by KARI (Korea) is planned to be launched on geostationary orbit in 2008 (KORDI report, 2003). Along with these instruments, the high-resolution sensors that are specifically developed for land applications are also used for deriving ocean parameters (Alfoldi, 1978; Collins and Pattiaratchi, 1984; Doxaran *et al.*, 2002).

Retrieval of ocean color information from these imageries is based on three different approaches: empirical, semi-empirical or semi-analytic and purely analytical. The empirical algorithms relay on statistical relationships between the upward radiance at the sea surface and the quantity of interest, while the later two cases are purely or partially relaying on optical properties in the water (Gordon and Morel, 1983; Ahn, 1999). Since the last two and half decades, many algorithms were derived empirically to estimate chlorophyll-a concentrations in Case-I waters (Morel and Prieur, 1977; Morel; 1988; Mitchell and Kiefer, 1988; Lee *et al.*, 1998). However, the accuracy of these algorithms is largely depending on the precise in-situ measurements, which are often caused by several factors including the abnormal sky light dispersion and sea surface reflection during the measurements.

Recently, the improvements in understanding the relationship between remote sensing reflectance (R_{rs}) and inherent optical properties (IOP) such as backscattering to absorption coefficients ratio [$b_b/(a + b_b)$] (Morel and Prieur, 1977) has resulted in the development of semi-empirical or semi-analytical algorithms to derive the constituents' concentrations from the oceanic waters (Carder *et al.*, 1999; Ahn, 1999; Bricaud *et al.*, 1998; Sathyendranath *et al.*, 2001; Loisel *et al.*, 2001; Garver and Siegel, 1997; McClain 1998). Compared to the purely empirical algorithms, semi-analytical algorithms are more accurate and reliable (Lee *et al.*, 1998). To derive pigment concentrations from the ocean, the blue/green ratio of radiances or remote reflectances is generally used in most of the bio-optical algorithms because chlorophyll absorbs more blue light than green and thus the ratio at these two wave bands decreases when the chlorophyll concentration increases. For instance, the phytoplankton pigment concentration in the open oceanic waters was derived from the empirical algorithms in which the relationship between

the ratios of radiances at CZCS shorter wave bands ($L_{wN}443/L_{wN}550$) to chlorophyll concentrations was established (Gordon *et al.* 1983). However, this ratio often yields more errors for high chlorophyll concentrations because of the low sensitivity of the blue wavelength (443nm) at higher concentrations (Bricaud *et al.*, 1999; Esaias *et al.*, 1998). To over come such errors, SeaWiFS Ocean Chlorophyll-2 and Ocean Chlorophyll-4 algorithms use the ratios of remote reflectances, $R_{rs}(490)/R_{rs}(555)$ and $R_{rs}(443)/ R_{rs}(555)$, $R_{rs}(490)/R_{rs}(555)$ and $R_{rs}(510)/R_{rs}(555)$ respectively (Reilly *et al.*, 1998). For the retrieval of suspended sediment concentrations, algorithms are based on the use of green waveband, which is highly sensitive to suspended particulate matter (Ahn *et al.*, 2001).

The Multi-spectral Camera (MSC) on Kompsat-2 satellite is expected to make significant contributions to the enhanced understanding of the complex interactions between physical, chemical, biological and geological processes in the coastal oceans. The present study aims to (1) the derivation and comparison of broad and narrow band algorithms for the retrieval of ocean color information from MSC on KOMPSAT-2 satellite, (2) the comparison of MSC algorithms with Landsat-5 TM (Thematic Mapper) algorithms because of having similar spectral characteristics, and (3) the implementation of Case-2 water algorithm on TM imagery for mapping the distribution of suspended sediments in the southwest sea of Korea.

2. Materials and Methods

1) Data

The data are from the in-situ and laboratory measurements consisting of remote sensing reflectance, chlorophyll (chl), suspended sediments (SS), and dissolved organic matter (DOM). The optical measurements were carried out by using a portable hyperspectral radiometer (Analytical Spectral Devices, ASD Inc.) with the spectral range of 350-1050nm. The five water leaving radiance spectra [$L_{wT}(\lambda)$] are averaged and corrected for the sky light reflection and the air-sea effects [$L_w(\lambda) = L_{wT}(\lambda) - F_r(\lambda)*L_{sky}(\lambda)$]. The values of $L_{sky}(\lambda)$ were obtained from the sky radiometer and F_r value was assumed to be constant 0.025 (Austin, 1974). In fact, F_r varies with viewing geometry, sky conditions (clear, partially and densely cloudy), sea surface roughness due to wind, and is wavelength-dependent under a cloudy sky (Mobley, 1999). The chlorophyll and suspended sediment concentrations were determined from the water samples collected simultaneously with the optical measurements. The remote sensing reflectance spectra from these measurements are used for the purpose of comparing with model-generated reflectances of Case-I and Case-II waters. Two models presented here include the Rrs model developed by Ahn (1999), which generates the R_{rs} values from 400nm to 700nm for different chlorophyll and suspended sediment concentrations, and spectral band model that converts the model generated R_{rs} values to the equivalent R_{rs} spectra at MSC and TM spectral bands. The theoretical background of these models is described in the following sections.

2) Conceptual Background of Remote Sensing Reflectance Model

A remote sensing model [R_{rs}] was developed by Ahn (1999) in order to extract the constituents' concentrations of interest in seawater. The 'R_{rs} model' works as functions of inherent optical properties such as absorption [$a(\lambda)$] and backscattering [$b_b(\lambda)$] coefficients of six water components including water, phytoplankton (chl), dissolved organic matter (DOM), suspended mineral particles (SS) heterotropic organism (he) and an unknown component, possibly represented by bubbles or other particulates unrelated to the first five

components. For the simplicity of the model, we assume clear skies, the sun position always at noon, satellite-viewing angle within 20 degree from nadir and no sun glint. According to Morel and Prieur (1977), the irradiance reflectance (R) can be related to inherent optical properties of seawater such as total beam absorption (Σ_{ai}) and total backscattering coefficients (Σ_{bi}) as follows

$$R(0^-) = \frac{\Sigma b_{bi}}{\Sigma a_i + \Sigma b_{bi}} \quad (1)$$

The function f is dependent on the radiance distribution within the subsurface light field and on the volume scattering function, $\beta(\theta)$, of particles in seawater. The irradiance reflectance, $R(0^-)$, just beneath the surface can be defined as;

$$R(0^-) = \frac{E_u(0^-)}{E_d(0^-)} = \frac{Q_u L_u(0^-, \theta, \varphi)}{(1-\rho)E_d(0^+)} \quad (2)$$

where, $L_u(0^-, \theta, \varphi)$ is the upwelling radiance in the direction of zenith (θ) and azimuth (φ) angles just beneath the surface. $E_u(0^-)$ and $E_d(0^-)$ are the upwelling and downwelling irradiances at null depth denoted by 0^-. L_u denotes the upwelling radiance and the bi-directional factor Q_u is not a constant but a function of depth and direction (θ, φ). According to Austin (1980), π must be replaced by a factor close to 5 if L_u is in the nadir direction. Under the above assumptions, L_u is then no longer a function of zenith and azimuth angles. To convert E_d (0^-) to E_d (0^+), the following relationship is used [E_d (0^-) = (1 - ρ) E_d (0^+). where ρ is averaged Fresnel reflectance at the air-sea interface and it will vary with sky conditions, sun elevation and sea surface state (wind speed). According to Morel and Gentili (1996), ρ values occur within the range of 4-5%. But our in situ measurements reveal that it varies from 5% under clear sky to 15% under cloudy conditions. In the present study, we adopt a ρ value of 5% for clear sky. In a strict sense, the R_{rs} cannot be called "reflectance" because of having the units of pf sr^{-1} to link the irradiance reflectance to the remote sensing reflectance by the following relation,

$$R_{rs} = \frac{L_w}{E_d(0^+)} = \frac{L_{wN}}{F_o} \quad (3)$$

Where L_w is the water leaving radiance [= $L_u(0^+)$] and L_{wN} is the normalized water leaving radiance. F_o is the extraterrestrial solar irradiance. Using the radiance transmitted through the air-sea interface [Fresnel n^2 Law; and n = 1.34 according to Gordon and Morel (1983)], the L_w is expressed as follows,

$$L_w = 0.545\, L_u(0^-) \text{ (or) } L_u(0^-) = 1.83\, L_w \quad (4)$$

By assembling the equations (1), (2), (3) and (4), we can obtain the remote sensing reflectance by the following expression,

$$R_{rs} = \frac{1}{1.93}\frac{f}{Q_u}\frac{\Sigma b_{bi}}{(\Sigma a_i + \Sigma b_{bi})} \quad (5)$$

Where f/Q_u is a non-constant environmental factor and f is directly proportional to Q_u (Zaneveld, 1995). These two quantities follow similar trends with changing sun-angle. The range of variability of f/Q_u is less than that of the two individual parameters f and Q (Morel and Gentili, 1996). According to their results, f/Q_u ranges from 0.075 to 0.095 for the various optical properties. In considering the sensor-viewing angle (10-20 degree from nadir), a value of 0.085 can be adopted and thus the equation (5) becomes,

$$R_{rs} = 0.044\frac{\Sigma b_{bi}}{(\Sigma a_i + \Sigma b_{bi})} \quad (6)$$

The model demonstrated here is primarily used in the present study to generate R_{rs} spectra, which will later be used in the MSC and TM band models. The R_{rs} spectrum values are generated from 400nm to 700nm at 2nm intervals using only three components; chlorophyll (chl), non-chlorophyllous particles (NC), and dissolved organic matter (DOM). To generate the R_{rs} spectrum from equation (6), the total backscattering and absorption coefficients are decomposed into six in-water components as follows,

$$R_{rs} = 0.044 \frac{b_{bw}+b_{bph}+b_{bss}+b_{bhe}+b_{bdom}+b_{b?}}{b_{bw}+b_{bph}+b_{bss}+b_{bhe}+b_{bdom}+b_{b?}+a_w+a_{ph}+a_{ss}+a_{he}+a_{dom}} \quad (7)$$

Where, the subscripts denote absorption and backscattering coefficients of seawater (w), phytoplankton (ph), suspended sediment matter (SS), heterotropes (he), dissolved organic matter (DOM) and unknown components (?), which are possibly represented by pubbles, or other particulates unrelated to the first five components (Stramski, 1994; Ahn, 2000). In the model, the backscattering coefficient of unknown components was estimated using Ahn's (2000) method. Since the optical properties of suspended mineral particles in the seawater are poorly understood, we followed the optical properties of loess from previous work carried out by Ahn (1990). The backscattering coefficients of DOM and absorption coefficients of unknown components are not included in this study, as they are considered negligible for purposes of these computations. In addition, the absorption and backscattering coefficients for components are separated to their specific absorption (a*) and backscattering coefficients (b_b*), and concentration [<i>] [i.e. $a_i = a_i^* \times$ <i> and $b_{bi} = b_{bi}^* \times$ <i>] (Ahn, 1999). Table 1 shows the Case-I and Case-II water component criteria adopted to generate the remote sensing reflectance for this study purpose.

3) Spectral Band Model

The spectral band model is developed for converting the model generated R_{rs} values to the equivalent remote sensing reflectances at the MSC and TM bands. These reflectances are used in the empirical relationships to derive the <chl> and <SS> algorithms, which will retrieve the concentrations of chlorophyll [mg/m^3] and suspended particulate matter [g/m^3] from the spectral ratios of remote sensing reflectances or a single band reflectances in the visible wavebands of the TM and MSC. The general expressions of the Case-I (chlorophyll) and Case-II (suspended sediment) water algorithms are given as follows,

Table 1. Criteria adopted for modeling remote sensing reflectances for Case-I and Case-II waters.

Water components	Case-I water	Case-II water
<chl> (mg/m^3)	0.1 ~ 30	0.5 ~ 10
<SS> (g/m^3)	0.1 ~ 4	2 ~ 100
DOM (m^{-1})	0.01 ~ 0.3	0.1 ~ 1.0

$$<chl>\ [mg/m^3] = \alpha[X]^{\beta} \quad (8)$$

$$<SS>\ [g/m^3] = \alpha[R]^{\beta} \quad (9)$$

where α and β are regression coefficients and X is the spectral ratio of remote sensing reflectance [$R_{rs}(\lambda_1)$/ $R_{rs}(\lambda_2)$] in the blue and green wave bands respectively. R is the remote sensing reflectance at TM or MSC band2. Since the MSC and TM wave bandwidths are much greater than the available ocean color sensors, the R_{rs} spectral values generated at 2nm intervals by Ahn's model are converted to the equivalent MSC and TM band reflectances, [R_{rs}(MSC band1), R_{rs}(MSC band2), R_{rs}(MSC band3)] and [R_{rs}(TM band1), R_{rs}(TM band2), R_{rs}(TM band3)] and to the center wavelengths (2nm interval), [R_{rs}(MSC band1-centre), R_{rs}(MSC band2-centre), R_{rs}(MSC band3-centre)] and [R_{rs}(TM band1-centre), R_{rs}(TM band2-centre), R_{rs}(TM band3-centre)]. The normalized spectral responsivity (unit less) values of the MSC and TM wavebands are used in the spectral band model for the purpose of this conversion (Figs. 1a-d and Table 2). These spectral responsivities were determined by the combined responses of all path mirrors (primary, secondary, scan line corrector, scanning etc.), the spectral filters, and the individual detectors. Thus, the equations (8) and (9) can be changed according to the TM and MSC band reflectances as follows,

$$<chl>\ [mg/m^3] = \alpha\left[\frac{\overline{B_1}(\lambda)}{\overline{B_2}(\lambda)}\right]^{\beta} \quad (10)$$

$$<SS>\ [g/m^3] = \alpha\left[\overline{B_2}\right]^{\beta} \quad (11)$$

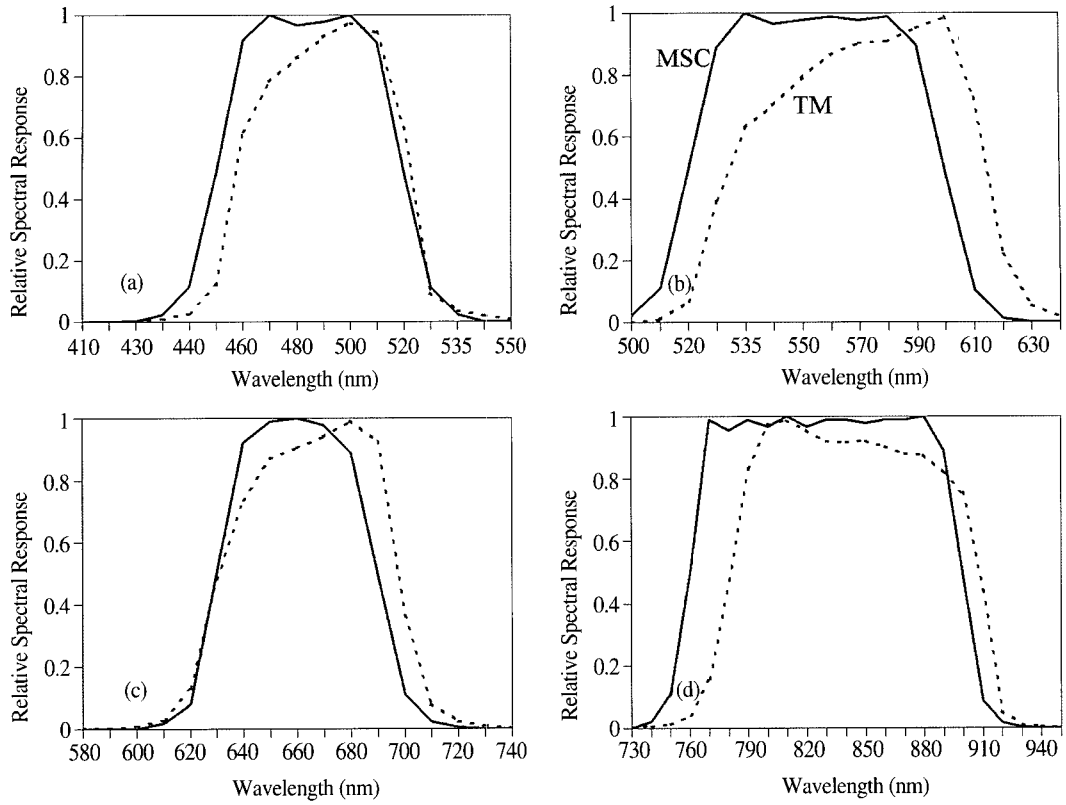

Figs. 1a-d. Normalized spectral responsivity (unitless) of the KOMSAT-2 Multi-Spectral Camera and Landsat-5 Thematic Mapper bands.

Table 2. Characteristic features of the Landsat-5 TM and Kompsat-2 MSC bands and their advantages for monitoring the highly dynamic coastal oceanic environmental parameters.

Spectral Band	Wavelength (μm)	Spatial Resolution (m)	Description	Characteristics
1	TM: 0.45~0.52 MSC: 0.45~0.52	30 4	Blue	Pigment absorption
2	TM: 0.52~0.60 MSC: 0.52~0.60	30 4	Green	Pigment and particles scattering
3	TM: 0.63~0.69 MSC: 0.63~0.69	30 4	Red	Pigment absorption
4	TM: 0.76~0.90 MSC: 0.76~0.90	30 4	Near infrared	Atmospheric correction

where $\overline{B_1}(\lambda)$ and $\overline{B_2}(\lambda)$ are the weighted R_{rs} values of the TM or MSC wavebands, $B_1(\lambda)$ and $B_2(\lambda)$ respectively. It can be modeled by the following equation,

$$\overline{B}(\lambda) = \frac{\sum_{j=1}^{n} S(\lambda_j) \times R_{rs}(\lambda_j)}{\sum_{j=1}^{n} S(\lambda_j)} \qquad (12)$$

where $S(\lambda_j)$ and $R_{rs}(\lambda_j)$ are the spectral responsivity and remote sensing reflectance at a given wavelength interval (λ_j) in each TM or MSC wavebands. The empirical algorithms are then established from the relationships between the weighted R_{rs} and the constituents' concentrations. Doxaran *et al.* (2002)

adopted a similar approach to analyze SPOT data for quantifying suspended particulate matter concentrations in the turbid estuarine waters of Gironde estuary, southwest France.

3. Results and Discussion

1) Comparison of Model-Derived and In-Situ Remote Sensing Reflectances

Using equation (6), a large number of remote sensing reflectances were generated for a diverse range of constituents' concentrations present in Case-I and Case-II waters. Fig. 2a shows model-derived remote sensing reflectance spectra for high chlorophyll concentrations [<chl> = 22 - 100 mg/m^3; <SS> = 0.7 - 2 g/m^3; DOM (400) = 0.03 - 0.15 m^{-1}]. The shape of these spectra is nearly in good agreement with that of in-situ spectra from the Jin-hae bay [<chl> = 43 - 71 mg/m^3; <SS> = 6.7 - 11 g/m^3; 0.1 - 0.7 m^{-1}] (Fig. 2b). In both spectra, the increased reflectance in the green region between 515nm and 600nm can be attributed to the phytoplankton, which, being refractive particles, increase scattering at these wavelengths. A progressive decrease in the measured R_{rs} values between 490nm and 540nm results from both high concentrations of DOM and pigments, which tend to increase absorption, and therefore reduced reflectance, at the blue and lower part of the green spectrum (Fig. 2b) (Morel and Prieur, 1977). Thus for estimating pigment concentrations, ocean color algorithms take advantage of the decreased reflectance in the blue (440-490nm) and the increased reflectance in the green region (545-560nm), by working in terms of the ratios in these two wave bands (Kirk, 1983; Gordon and Morel, 1983). The values of these two bands ratio decreases as the chlorophyll concentration increases. In contrast, the absorption feature between 440-490nm is not distinct at low chlorophyll concentrations [<chl> = 0.5 -3 mg/m^3; <SS> = 0.2- 1.5 g/m^3; DOM (400) = 0.02 - 0.06 m^{-1}] (Fig. 2c). However, a small deflection at 443 nm allows the reflectance ratio at 443 and 555nm [R_{rs}(443)/ R_{rs}(555)] that can be effectively used for estimating chlorophyll concentration in the ocean waters. It is interesting to see another peak around 685nm that arises from the sun-induced chlorophyll fluorescence signal from the ocean (Neville and Gower, 1977; Doerffer, 1981) (Figs. 2a and b). Previous studies have shown that the position and magnitude of this peak changes with respect to increasing chlorophyll concentrations (Kishino *et al.*, 1986; Gitelson, 1992). At low chlorophyll concentrations, the remote sensing reflectance spectra do not exhibit this peak around 685nm (Fig. 2c).

Similarly, a large number of remote sensing reflectance spectra (N=500) were also generated for a diverse range of suspended sediment concentrations [<chl> = 0.5 - 10 mg/m^3; <SS> = 10 - 100 g/m^3; DOM (400) = 0.1 - 1 m^{-1}] (Fig. 2d). It is apparent that the model-derived reflectance spectra compare very well with in-situ spectra collected around the Jin-do and Wan-do coastal waters during September and October 1998 (Fig. 2e). The in-situ spectra correspond to the suspended sediment concentrations from 3 - 120 g/m^3. These areas are always subject to high turbidity resulting from the process of sediment resuspension due to strong tidal currents (Ahn *et al.*, 2004). The suspended sediment particulate matters increase the backscattering more than the absorption coefficient towards longer wavelengths (Ahn, 1990), and therefore the reflectance values above the water surface increased with increasing SS concentrations at all wavelengths from 400 to 700nm (Figs. 2d and e).

2) Derivation of Empirical Algorithms for TM

Equation (12) transformed the model-derived R_{rs} to

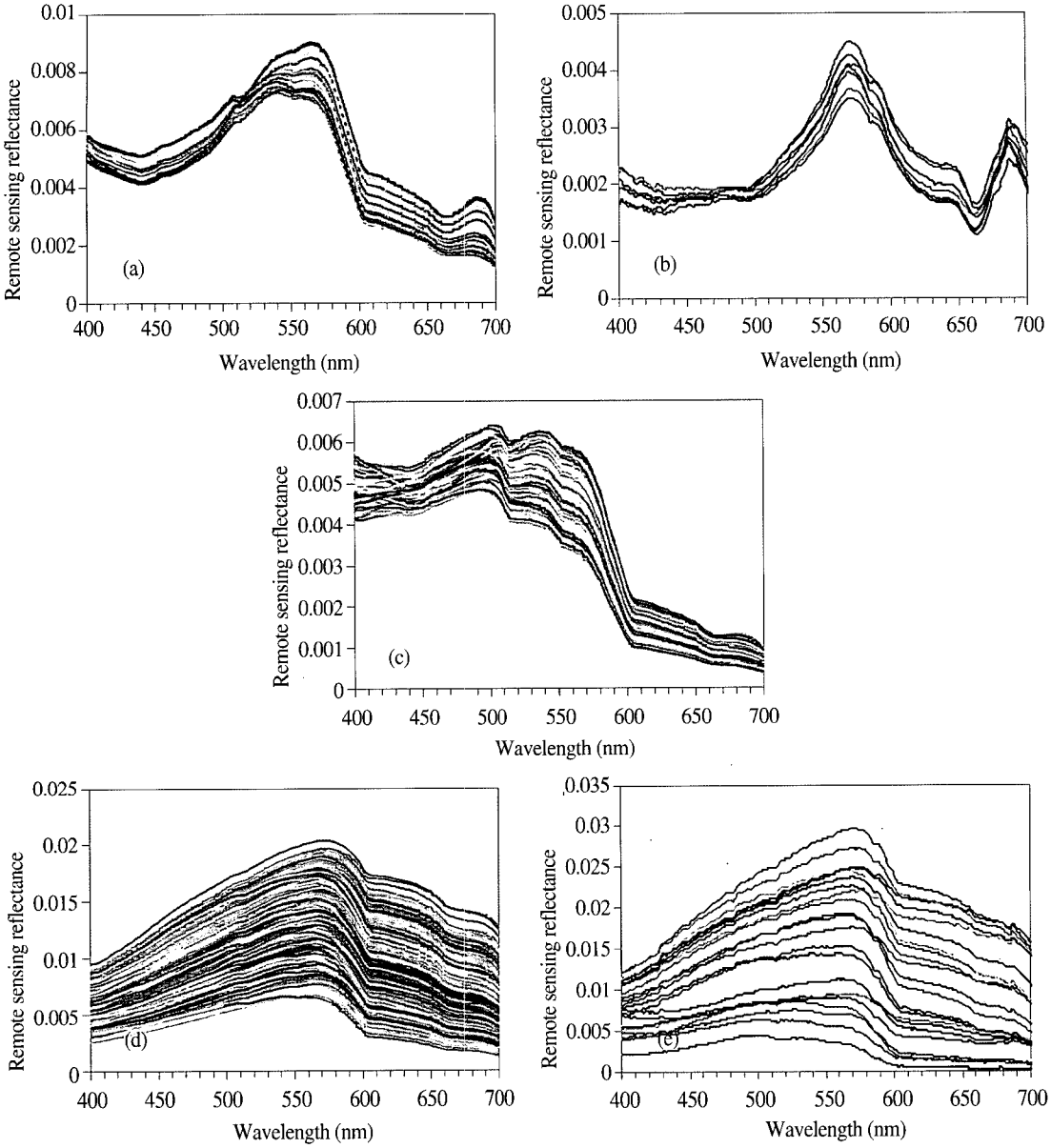

Figs. 2a-e. Comparison of modeled and in-situ remote sensing reflectance (R_{rs}) spectra in the spectral range between 400 and 700nm. (a) Modeled R_{rs} spectra of Case-I waters [<chl> = 22 -100 mg/m^3; <SS> = 0.7- 2 g/m^3; DOM (400) = 0.03 - 0.15 m^{-1}], (b) In-situ R_{rs} spectra of red-tide waters of the Jin-Hai bay during 8 Aug. 1999 [<chl> = 43 -71 mg/m^3; <SS> = 6.7- 11 g/m^3], (c) Modeled R_{rs} spectra for low chlorophyll concentrations [<chl> = 0.5 -3 mg/m^3; <SS> = 0.2- 1.5 g/m^3; DOM (400) = 0.02 - 0.06 m^{-1}], (d) Modeled R_{rs} spectra of highly turbid waters [<chl> = 0.5 -10 mg/m^3; <SS> = 10- 100 g/m^3; DOM (400) = 0.1 - 1 m^{-1}], (e) In-situ R_{rs} spectra from the Jin-do and Wan-do coastal waters during Sep. and Oct. 1998 [<chl> 0.7-1.2 mg/ m^3; <SS> = 3- 120 g/m^3].

the equivalent remote reflectances at the three TM wave bands [R_{rs}(TM1), R_{rs}(TM2) and R_{rs}(TM3)]. Fig. 3a represents spectral variation of remote reflectances as a function of TM wavebands for different chlorophyll concentrations from 4.1 to 31 mg/m^3. It is observed that the R_{rs} values decrease progressively toward the blue

and red wavebands that correspond to the maximum absorption by chlorophyll concentrations. The reflectance maxima occur in the green waveband centered at 560nm, where high backscattering by pigments is evident in this waveband (Morel and Prieur, 1977). On the other hand, Fig. 3b shows the remote sensing reflectance spectra for different concentrations of suspended sediment matter (18.8~88.7 g/m^3). One should note that the band 2 is highly sensitive to changes in backscattering by suspended sediment particles than the blue and red wavebands. Ahn *et al.* (2001) pointed out that the longer part of the green and lower part of the red wavebands are highly useful to derive SS

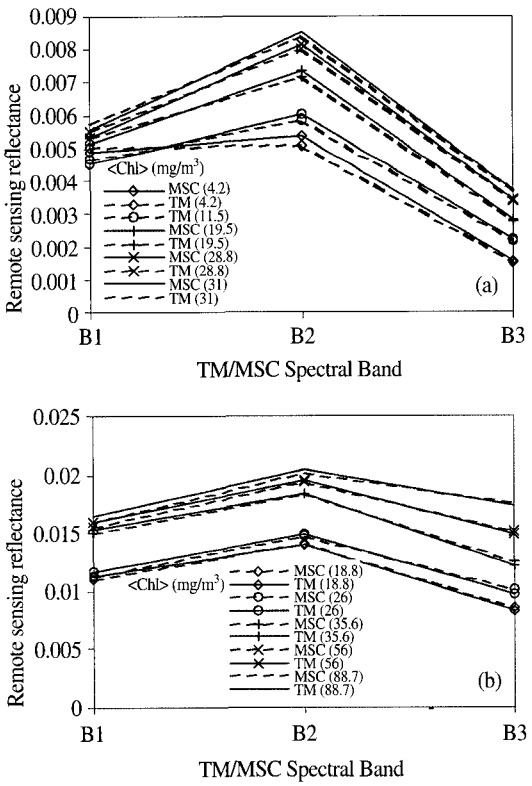

Fig. 3. Comparison of the modeled remote sensing reflectance spectra [(R_{rs} (λ))] of TM and MSC wavebands for different chlorophyll concentrations [<chl> (mg/m^3)]. (b) Comparison of the modeled remote sensing reflectance spectra [(R_{rs} (λ))] of TM and MSC wavebands for different suspended sediment concentrations [<SS> (g/m^3)].

concentrations in a highly turbid waters. Similarly, Doxaran *et al.* (2002) noticed that the R_{rs} values increase progressively from green to red (500-700nm) and become stable between 750 and 950nm for high SS concentrations.

In this study, statistical regression analysis of remote reflectance data was performed against the chlorophyll and suspended sediment concentration to derive <chl> and <SS> algorithms for ocean color interpretation of the TM and MSC imageries. The empirical relationship between the spectral ratio of remote sensing reflectance [R_{rs}(TM1)/R_{rs}(TM2)] and chlorophyll concentrations allows us to derive the equation for estimating the chlorophyll concentration from the TM broad wavebands (Fig. 4a). The regression formula can be expressed as follows,

$$<chl>\ [mg/m^3] = 4.36x^{-4.63} \quad (13)$$

where x is the broadband ratio R_{rs}(TM1)/R_{rs}(TM2). The determination coefficient for log-transformed data, r^2 = 0.90 and the number of observations, n = 500. The center waveband relationship, R_{rs}(TM Band1-centre)/ R_{rs}(TM Band2-centre) verses chlorophyll concentrations is almost similar with the broadband relationship, though a small discrepancy may be attributed to the fact of the bandwidth (Fig. 4a). The regression equation obtained for center wavelength ratio is given as follows

$$<chl>\ [mg/m^3] = 2.34x^{-4.22} \quad (14)$$

where x is the center band ratio of TM band 1 and 2. The determination coefficient is r^2 = 0.91. The statistical comparison based on log-transformed data is due to the fact that the log-transformed data is normally distributed than the untransformed data (O'Reilly *et al.* 1998). The regression slope and intercept and the determination coefficient (r^2) provided a numerical index of model performance. A good correlation occurred in both cases, with a small discrepancy between the broad and narrow wavebands (centre) relationships.

Similarly, statistical regression analysis of the single

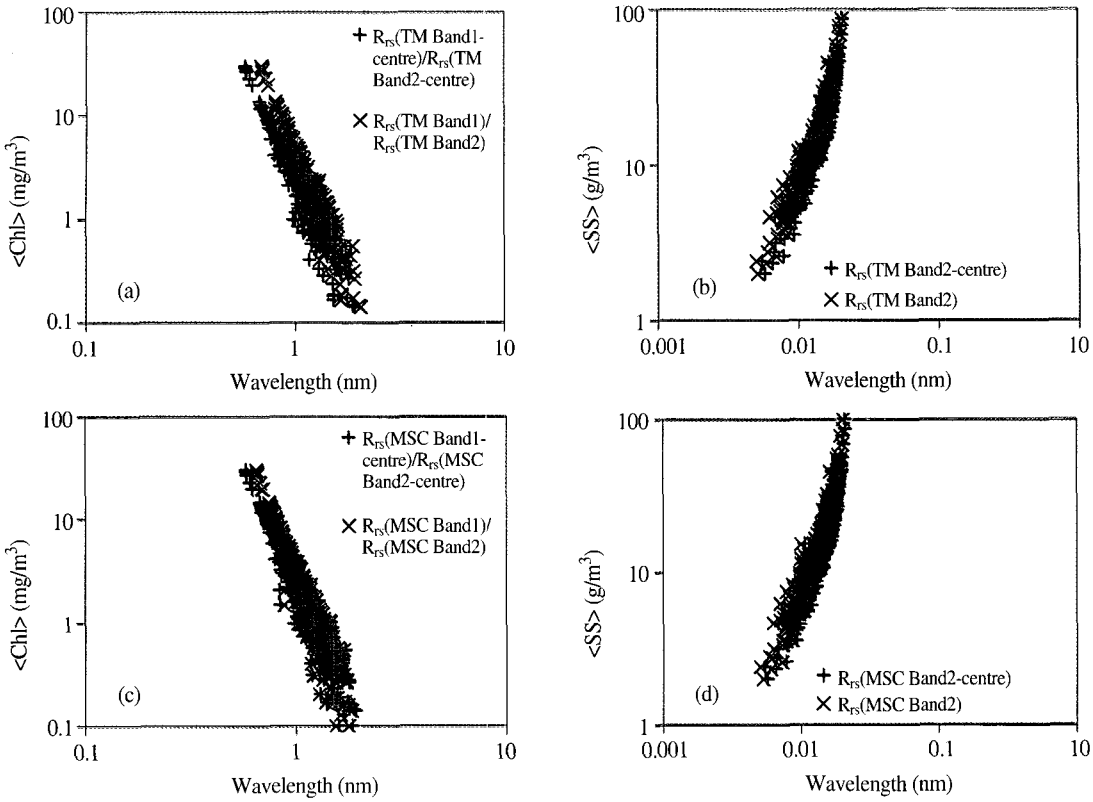

Figs. 4a-d. Relationships between remote sensing reflectances and constituents concentrations. (a) R_{rs}(TM Band1-centre)/R_{rs}(TM Band2-centre) and R_{rs}(TM Band1)/R_{rs}(TM Band2) verses chlorophyll concentrations [<chl> (mg/m^3)], (b) R_{rs}(TM Band2-centre) and R_{rs}(TM band2) verses suspended sediment concentrations [<SS> (g/m^3)], (c) R_{rs}(MSC Band1-centre)/R_{rs}(MSC Band2-centre) and R_{rs}(MSC Band1)/R_{rs}(MSC Band2), verses chlorophyll concentrations [<chl> (mg/m^3)], (d) R_{rs}(MSC Band2-centre) and R_{rs}(MSC band2) verses suspended sediment concentrations [<SS> (g/m^3)]. Here, Band1 or Band2-centre denotes narrowband, and Band1 or Band2 stands for broadband.

band raflectances was performed against the suspended sediment concentration (Fig. 4b). The regression equation for the broadband relationship [R_{rs}(TM band2 verses <SS> concentrations) is expressed as follows

$$<SS>\ (g/m^3) = 0.99e^{199.9x} \quad (15)$$

with the determination coefficient, $r^2 = 0.93$. The term 'x' refers to R_{rs}(TM band2). The equation for the center band relationship [R_{rs}(TM Band3-centre) verses <SS> concentrations] is defined as

$$<SS>\ (g/m^3) = 0.85e^{199.7x} \quad (16)$$

with the determination coefficient, $r^2 = 0.91$, where x is the R_{rs}(TM Band2-centre). For both cases, the total number of observations, n = 500. The exponential form is due to the fact that the total suspended sediment concentration corresponds best with an exponential, rather than linear function of radiance or reflectance in this system (Klemas *et al.*, 1974). It is worth noting that the broadband relationship gave the best fit with r^2 = 0.93 compared to the center band relationship [r^2 = 0.91]. To estimate the SS concentration, we used a single band reflectance rather than the spectral ratio of remote sensing reflectances at two wavebands (Doxaran *et al.*, 2002) because the two-band ratio algorithm makes very poor performance in coastal waters, where the DOM absorption is inevitably intermingled with blue

waveband (Ahn *et al.*, 2001). The single band approach is consistent with the previous studies carried out by Klemas *et al.* (1974) and Munday and Alfoldi (1979).

3) Derivation and Comparison of Empirical Algorithms for MSC

Fig. 3a compares TM and MSC band reflectances for various chlorophyll concentrations 4.2~31 mg/m^3. It is seen that having a high sensitivity of MSC bands resulted in slightly increased values of remote sensing reflectance than TM. In both spectra, the absorption by pigments is very distinct in blue and red wavebands while scattering by organic particles is representative of green band of these sensors. Therefore, the decreased reflectance in the blue and increased reflectance in the green can be effectively adopted in the empirical algorithms by taking the ratio of these two wavebands. A similar trend can be observed in R_{rs} spectra of TM and MSC that increase with increasing suspended sediment concentrations 18.8~88.7g/m^3 as shown in Fig. 3b. Note that there exists a small difference in R_{rs} spectra of case-II waters compared to Case-1 water reflectances. Fig. 4c shows the relationship between the spectral ratios remote reflectances, [R_{rs}(MSC Band1)/ R_{rs}(MSC Band2)] and [R_{rs}(MSC Band1-centre)/ R_{rs}(MSC Band2-centre)] and chlorophyll concentrations [<chl> (mg/m^3)]. It appears that the scatters of the broad and narrow wavebands of MSC as a function of chlorophyll concentrations become closer than that of TM, suggesting that MSC bands reflectances are more sensitive to varying constituent's concentrations than TM band reflectances. The regression equation for broadband relationship is given as follows,

$$<chl>\ [mg/m^3] = 2.93x^{-4.89} \quad (17)$$

The determination coefficient for the log-transformed data is $r^2 = 0.90$. Similarly, the empirical formula for the narrow (centre) waveband derived is as

$$<chl>\ [mg/m^3] = 2.37x^{-4.25} \quad (18)$$

with $r^2 = 0.91$, where x defines the spectral ratios of broad and narrow wavebands respectively, [R_{rs}(MSC Band1)/ R_{rs}(MSC Band2)] and [R_{rs}(MSC Band1-centre)/R_{rs}(MSC Band2-centre)]. For each case, the total number of observations, N = 500. The equations are representative of power law functions used to relate R_{rs} ratios to chlorophyll concentration due to the relative ease of derivation of model parameters using a simple linear regression of log-transformed data (Smith and Baker, 1982). Similarly, <SS> algorithms were derived from the relationships between [R_{rs}(MSC Band2)] and [R_{rs}(MSC Band2-centre)] and SS concentrations (Fig. 4d). The followings are the empirical equations for R_{rs}(MSC Band2) and R_{rs}(MSC Band2-centre) respectively.

$$<SS>\ (g/m^3) = 0.89e^{205.7x},\ [r^2 = 0.92] \quad (19)$$

$$<SS>\ (g/m^3) = 0.81e^{202.4x},\ [r^2 = 0.91] \quad (20)$$

where x is the broad or narrow band reflectance at MSC band 2. The performance of broadband SS algorithm is seemingly better than the centerband algorithm that has low correlation coefficient value $r^2 = 0.91$.

Since these algorithms relay on model parameters, they may have several advantages over purely empirical ones because the empirical algorithms derived from statistical regression of radiance verses chlorophyll require large set of in situ data (Reilly *et al.*, 1998) to relate the ratios of remote sensing reflectances [R_{rs} (λ)] or normalized water leaving radiance [L_{wN} (λ)] (Gordon, 1983), to chlorophyll concentration. The accuracy of these algorithms is largely depending on the precise data from in situ and laboratory measurements that are often caused by several factors as mentioned earlier. In view of band combinations, the ratio R_{rs}443/R_{rs}550 will be very useful at low chlorophyll concentrations, <chl> <3mg/m^3. At higher concentrations, 443nm band is essentially influenced by both pigment and DOM absorptions, leading to produce large errors in highly productive waters. To over come this problem, NASA

OC2 algorithm uses the band ratio, $R_{rs}(490)/R_{rs}(555)$ for a diverse range of waters (Reilly *et al.* 1998). Crucially, this algorithm yields large errors at low chlorophyll concentrations (Lee *et al.*, 1998; Sathyendranath *et al.*, 2001; Yoo *et al.*, 2000; Burenkov *et al.*, 2000).

Thus to improve the accuracy of <chl> estimates, many algorithms rely on more than two bands. For example, OC4 is a four band algorithm using $R_{rs}(443)/R_{rs}(555)$, $R_{rs}(490)/R_{rs}(555)$, or $R_{rs}(510)/R_{rs}(555)$, the OCTS-C model is a power-law formulation using the sum of $L_{wN}(520)+L_{wN}(565)$ over $L_{wN}(490)$, the CalCOFI a three band multiple regression algorithm using band ratios $R_{rs}(490)/R_{rs}(555)$ and $R_{rs}(510)/R_{rs}(555)$, the functional form of CalCOFI four-band algorithm is using $R_{rs}(443)/R_{rs}(555)$ and $R_{rs}(412)/R_{rs}(510)$ (Reilly *et al.*, 1998). Analyzing the performance of these algorithms implies that more number of bands results in accurate estimates of chlorophyll concentrations in ocean waters. Thus, the broadband algorithm having a small difference with the narrowband algorithm improves the signal to noise ratio and covers the spectral range of the aforementioned algorithms. Moreover, the effect of DOM absorption at MSC band1 could be comparatively lesser than that at narrow waveband. In case of the SS retrieval, the single and broadband algorithm could be more powerful than the band ratio and narrow band algorithms. The potential use of single band algorithms has already been demonstrated in different waters (Klemas *et al.*, 1974; Munday and Alfoldi; 1979; Ahn *et al.*, 2001).

4) Application

The application of broadband SS algorithm is demonstrated in highly turbid waters around the southwestern part of the Korean peninsula using Landsat-5 TM imagery acquired on 7 May 2000. Prior to the implementation of this algorithm, the TM image was corrected for the atmospheric effects with the Spectral Shape Matching Method (SSMM) developed by Ahn and Shanmugam (2004). Fig. 5 shows dynamic patterns of SS distributions around the Jin-do and Wan-do areas. SS concentration varies from 1~120 <SS> (g/m^3). Intricate and striking patterns of sediments that result from the process of sediment resuspension owing to strong tidal currents and bottom circulations are not interpretable with low spatial resolution imagery such as, SeaWiFS and AVHRR. The prediction of such highly dynamic SS patterns in the coastal regions can help in the determination of the rate and magnitude of sediment transport that impedes navigational and submarine practices in the southern Yellow Sea. From this study, it was found that application of SSMM and SS algorithm to the Landsat VIS/NIR imagery has proven highly useful in bringing out a clear picture about water column dynamics in the southwest coastal sea.

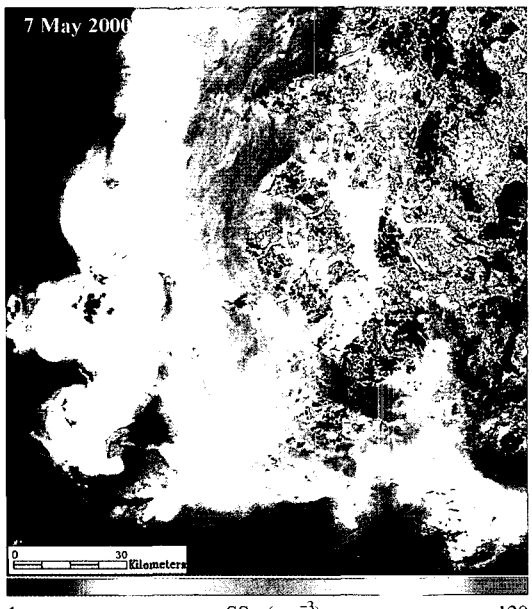

Fig. 5. The high resolution suspended sediment map obtained from the Landsat-5 TM imagery (7 May 2000) over southwest coastal waters of Korea by the implementation of SSMM and TM SS algorithm.

4. Conclusion

Multi-Spectral Camera (MSC) on Kompsat-2 satellite is expected to provide an enhanced understanding of the dynamics of small-scale coastal oceanic features such as red tide blooms, suspended sediments, eddies, meanders and other circulation patterns. Interpretation of these features is not feasible with the currently available coarse spatial resolution ocean color sensors that can only show some unpredictable signatures. To map and monitor such highly dynamic features in the coastal oceanic waters, broad and narrow band algorithms were derived from the statistical relationships established using a large data set generated by R_{rs} and spectral band models. These algorithms will be capable of deriving accurate information about the ocean color from MSC or TM imagery. The difference between the spectral ratios of remote sensing reflectances at narrow waveband [R_{rs}(MSC Band1-centre)/R_{rs}(MSC Band2-centre)] and broad waveband [R_{rs}(MSC Band1)/ R_{rs}(MSC Band2)] as functions of chlorophyll concentrations was significantly low. Thus, the broadband algorithm derived from the relationship between R_{rs}(MSC Band1)/R_{rs}(MSC Band2) and chlorophyll concentrations may have certain similarities with OC4, CalCOFI, OCTS-C because these algorithms rely on more than two wavebands. In contrast, the single band SS algorithms for TM and MSC appear to perform better than narrow band algorithms that have relatively low correlation with SS concentrations (r^2 = 0.91). The previous study indicated that the use of band ratio algorithms does not seem to be potential for the accurate retrieval of SS concentrations in the ocean waters. The model-derived remote sensing reflectance spectra were shown to be consistent with the in-situ data from turbid and other coastal waters. The potential use of the developed algorithms was also explored and demonstrated in highly turbid waters around the Jin-do and Wan-do bays using Landsat-TM imagery. The results suggest that these algorithms combined with SSMM can be very useful for mapping and monitoring coastal ocean environmental parameters using MSC and TM imageries. The applicability of these algorithms for various water types is not assessed in this study, therefore, we will plan in the future to evaluate the model and in-situ algorithms using TM and MSC images.

Acknowledgements

This research was supported by Ministry of Science and Technology (MOST) and Ministry of Maritime Affairs and Fisheries (MOMAF) under the KORDI contract No. PN 541-00 and PM 294-00.

References

Abbott, M. R. and D. B. Chelton, 1991. Advances in passive remote sensing of the ocean. *Reviews of Geophysics*, 29: 571-589.

Ahn, Y. H., 1990. Optical properties of biogeneous and mineral particles present in the ocean. Application: Inversion of reflectance. Ph.D thesis, Paris-VI University, France.

Ahn, Y. H., A. Bricaud, and A. Morel, 1992. Light backscattering efficiency and related properties of some phytoplankters. *Deep-Sea Research*, 39: 1835-1855.

Ahn, Y. H., 1999. Development of an inverse model from ocean reflectance. *Marine Technology Society Journal*, 33: 69-80.

Ahn, Y. H., 2000. Development of remote sensing reflectance and water leaving radiance models for ocean color remote sensing technique. *Journal of the Korean Society of Remote Sensing*, 16: 240-260.

Ahn, Y. H., J. E. Moon, and S. Gallegos, 2001.

Development of suspended particulate matter algorithms for ocean color remote sensing. *Korean Journal of Remote Sensing*, 17: 285-295.

Ahn, Y. H., P. Shanmugam., and S. Gallegos, 2004. Evolution of suspended sediment patterns in the East China and Yellow Sea. *Journal of the Korean Society of Oceanography*, 39, 26-34.

Ahn, Y. H. and P. Shanmugam, 2004. New methods for correcting the atmospheric effects in Landsat Imagery over turbid waters, 20(5): 289-305.

Alfoldi, T. T., 1978. water quality analysis by digital chromaticity mapping of Landsat data. *Canadian Journal of Remote Sensing*, 4: 108-126.

Austin, R. W., 1974. Inherent spectral radiance signatures of the ocean surface, In: Ocean color analysis. La Jolla, CA, Scripps Institute of Oceanography, pp.195.

Austin, R. W., 1980. Gulf of Mexico, ocean-color surface-truth measurements. *Boundary Layer Meteorology*, 18: 269-285.

Barale, V. and C. C. Trees, 1987. Spatial variability of the ocean color field in CZCS imagery. *Advances in Space Research*, 7: 95-100.

Bricaud, A., A. Morel, and L. Prieur, 1981. Absorption by dissolved organic matter of the sea (yellow substance) in the UV and visible domains. *Limnology and Oceanography*, 26: 43-53

Bricaud, A., A. Morel., M. Babin., K. Allali, and Claustre, 1998. Variation of light absorption by suspended particles with chlorophyll a concentration in oceanic (Case- 1) waters: Analysis and implications for bio-optical models, *Journal of Geophysical Research*, 103: 31,033-31,044.

Bricaud, A., A. Morel, and V. Barale, 1999. MERIS potential for ocean color studies in the open ocean. *International Journal of Remote Sensing*, 20: 1757-1769.

Burenkov, V. I., O.V. Korelvich., S. V. Sheberstov, and V. I. Vedernikov, 2000. Sub-satellite measurements of ocean color: validation of the SeaWiFS satellite scanner data. *Oceanology*, 40: 357-362.

Carder, K. L., F. R. Chen., Z. P. Lee, and S. K. Hawes, 1999. Semi-analytic Moderate-Resolution Imaging Spectrometer algorithms for chlorophyll-a and absorption with bio-optical domains based on nitrate depletion temperatures. *Journal of Geophysical Research*, 104: 5403-5421.

Collins, M. and C. Pattiaratchi, 1984. Identification of suspended sediment in ocean waters using airborne thematic mapper data. *International Journal of Remote Sensing*, 5: 635-657.

Doerffer, R., 1981. Factor analysis in ocean color interpretation. In: Oceanography from space, (Gower, J.F.R., ed), Plenum Press, NY, 339-345.

Doxaran, D., J. M. Froidefond., S. Lavender, and P. Castaing, 2002. Spectral signature of highly turbid waters. Application with SPOT data to quantify suspended particulate matter concentrations. *Remote Sensing of Environment*, 81: 149-161.

Esaias, W. E., M. R. Abbott., I. Barton., O. B. Brown., J. W. Campbell., K. L. Carder., D. K. Clark., R. H. Evans., F. E. Hoge., H. R. Gordon., W. M. Balch., R. Letelier, and P. J. Minnett, 1998. An overview of MODIS capabilities for Ocean science observations. *IEEE Transactions on Geoscience and Remote Sensing*, 36: 1250-1264.

Garver, S. A. and D. A. Siegel, 1997. Inherent optical property inversion of ocean color spectra and its biogeochemical interpretation: Time series from the Sargasso Sea. *Journal of Geophysical Research*, 102: 18,607-18,625.

Gitelson, A., 1992. The peak near 700nm on reflectance spectra of algae and water: relationships of its magnitude and position with chlorophyll concentration. *International Journal of Remote Sensing*, 13: 3367-3373.

Gordon, H. R., D. K. Clark., J. L. Mueller, and W. A. Hovis, 1980. Phytoplankton pigments from the Nimbus-7 coastal Zone Color Scanner: Comparisons with surface measurements. *Science*, 210: 63-66.

Gordon, H. R. and A. Morel, 1983. Remote assessment of ocean color for interpretation of satellite visible imagery: A review. Lecture notes on Coastal and Estuarine studies, M. Bowman (ed.), Spring-Verlag. pp.114.

Kirk, J. T. O., 1983. *Light and Photosynthesis in Aquatic Ecosystems*, Cambridge University Press, Cambridge, UK.

Kishino, M., S. Sugihara, and N. Okami, 1986. Theoretical analysis of the in situ fluorescence of chlorophyll-a on the underwater spectral irradiance. *Bulletein de la Societe Franco-Japanaise d' Oceanographie*, 24: 130-138.

Klemas, V., D. Bartlett., W. Philpot., R. Rogers, and L. Reed, 1974. Coastal and estuarine studies with ERTS-1 and Skylab. *Remote Sensing of Environment*, 3: 153-74. 152,162-3.

KORDI Report, 2003. Preliminary studies and the user requirements of the ocean payloads in geostationary orbit satellites, BSPK045-00-1536-1, Korea.

Lee, Z. P., K. L. Carder., R. G. Steward., T. G. Peacock., C. O. Davis, and J. S. Patch, 1998. An empirical algorithm for light absorption by ocean water based on color. *Journal of Geophysical Research*, 103: 27,967-27,978.

Loisel, H., D. Stramski., B. G. Mitchell., F. Fell., F. Fournier-Sicre., B. Lemasle, and M. Babin, 2001. Comparison of the ocean inherent optical properties obtained from measurements and inverse modeling. *Applied Optics*, 40: 2384-2397.

Mobley, C. D., 1999. Estimation of the remote sensing reflectance from above-sea surface. *Applied Optics*, 38: 7442-7455.

McClain, C. R., 1998. Ocean color chlorophyll algorithms for SeaWiFS. *Journal of Geophysical Research*, 103(24): 937-953.

Mitchell, B. G. and D. A. Kiefer, 1988. Chlorophyll a specific absorption and fluorescence excitation spectra for light limited phytoplankton. *Deep-Sea Research*, 35: 639-663.

Morel, A. and L. Prieur, 1977. Analysis of variations in ocean color. *Limnology and Oceanography*, 22(4): 709-722.

Morel, A., 1988. Optical modeling of the upper ocean in relation to its biogenous matter content (Case-I waters). *Journal of Geophysical Research*, 93: 749-10,768.

Morel, A. and B. Gentli, 1996. Diffuse reflectance of oceanic waters. III. Implication of bidirectionality for the remote sensing problem. *Applied Optics*, 35: 4850-4862.

Munday, J. C. and T. T. Alfoldi, 1979. Landsat test of diffuse reflectance models for aquatic suspended solids measurement. *Remote Sensing of Environment*, 8: 83-169, 145-6, 152-3.

Neville, R. A. and J. F. R. Gower, 1977. Passive remote sensing of phytoplankton via chlorophyll-a fluorescence. *Journal of Geophysical Research*, 82: 3487-3493.

O'Reilly, J. E., S. Maritorena., B. G. Mitchell., D. A. Seigel., K. L. Carder., S. A. Garver., M. Kahru, and C. McClain, 1998. Ocean color chlorophyll algorithms for SeaWiFS. *Journal of Geophysical Research*, 103: 24,937-24953.

Sathyendranath, S., G. Cota., V. Stuart., H. Maass, and T. Platt, 2001. Remote sensing of phytoplankton

pigments: a comparison of empirical and theoretical approaches. *International Journal of Remote Sensing*, 22: 249-273.

Smith, R. C. and K. S. Baker, 1982. Oceanic chlorophyll concentrations as determined by satellite (Nimbus-7 coastal zone color scanner). *Marine Biology*, 66: 269-279.

Stramski, D., 1994. Gas micropubbles: An assessment their significance to light scattering in quiescent seas. Ocean optics XII, J.S. Jaffe, editor, *Proc. Society of Photo-Optical Instrumentation Engineers*, Bellingham, 2258: 704-710.

Stumpf, R. P. and J. R. Pennock, 1991. Remote estimation of the diffuse attenuation coefficient in a moderately turbid estuary. *Remote Sensing of Environment*, 38: 182-191.

Yoo, S. J. and H. C. Kim, 2000. Validation of ocean color algorithms in the Ulleung Basin, East/Japan Sea. *Journal of the Korean Society of Remote Sensing*, 16: 315-325.